A Three-Terminal Switch Model of Constant On-Time Current Mode With External Ramp Compensation

Shuilin Tian, *Student Member, IEEE*, Fred C. Lee, *Life Fellow, IEEE*, Jian Li, Qiang Li, *Member, IEEE*, and Pei-Hsin Liu, *Student Member, IEEE*

***Abstract*—Multiphase constant on-time current-mode control based on pulse distribution structure is widely used in voltage regulator application for microprocessor. To minimize ripple cancellation effect, external ramp compensation is used in commercial products. However, external ramp will introduce dynamic to the system and stability margin will be suffered without considering its effect. This paper first studies the effect of external ramp by deriving small-signal transfer function based on describing function method. It is found that external ramp brings additional dynamic, with time constant related with switching period. Then, a simple equivalent circuit model based on three-terminal switch concept is proposed, which considers the effect of external ramp by adding an additional *R–L* branch. The equivalent circuit model can be reduced to previous unified three-terminal switch model when external ramp is zero and can be reduced to model of constant on-time voltage mode control when external ramp is much larger than inductor current ramp. The proposed three-terminal switch model is a complete model, which can be used to examine all transfer functions and is accurate up to half of switching frequency. The analytical transfer functions are provided for easy reference. The model is verified by SIMPLIS simulation and experimental measurement.**

***Index Terms*—Constant on-time current mode, external ramp compensation, three-terminal switch model.**

I. Introduction

MULTIPHASE constant on-time current-mode control based on pulse distribution structure is widely used in Voltage Regulator application for microprocessor [1]–[4]. The structure is shown in Fig. 1 and the steady-state waveform for a two-phase constant on-time current-mode control is shown in Fig. 2. The switch turn-off instant is determined by the on time and the switch turn-on instant is decided by the comparison of the total inductor current, the external ramp, and the control signal from feedback. The pulse distribution scheme sends the first turn-on instant to the first phase and the second turn-on instant to the second phase. By this way, the implementation is simple and it is capable of automatic interleaving between different phases. Compared with constant on-time voltage mode control, current-mode control can simplify the feedback design and improve dynamic performance [5], [6]. Compared with peak current-mode control structure, constant on-time current-mode control has better small-signal plant characteristic and, therefore, can achieve a wider bandwidth with sufficient phase margin [7], [8].

For single phase operation, external ramp compensation is not necessary as there is no current loop instability problem for constant on-time current-mode control [7], [8]. However, for multiphase operation, the structure based on pulse distribution structure suffers the ripple cancelation effect due to interleaving

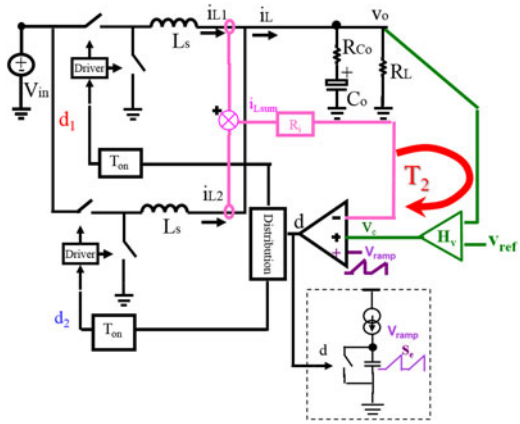

Fig. 1. Multiphase constant on-time current-mode structure based on pulse distribution with external ramp compensation [2], [3].

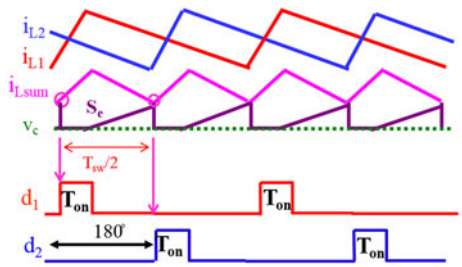

Fig. 2. Steady-state waveform for two-phase constant on-time current-mode structure based on pulse distribution with external ramp compensation [2], [3].

Manuscript received June 25, 2015; revised November 24, 2015 and September 29, 2015; accepted November 29, 2015. Date of publication December 11, 2015; date of current version May 20, 2016. Recommended for publication by Associate Editor Ting Qian.

S. Tian and J. Li were with the Bradley Department of Electrical and Computer Engineering, Center for Power Electronics Systems, Virginia Tech, Blacksburg, VA 24061 USA. They are now with Linear Technology, Milpitas, CA 95035-7417 USA (e-mail: tianshuilinpe@gmail.com; jianli04@vt.edu).

F. C. Lee and Q. Li are with the Bradley Department of Electrical and Computer Engineering, Center for Power Electronics Systems, Virginia Tech, Blacksburg, VA 24061 USA (e-mail: fclee@vt.edu; lqvt@vt.edu).

P.-H. Liu was with the Bradley Department of Electrical and Computer Engineering, Center for Power Electronics Systems, Virginia Tech, Blacksburg, VA 24061 USA. He is now with the Texas Instruments, Manchester, NH 03101 USA (e-mail: peihsin8@vt.edu).

Color versions of one or more of the figures in this paper are available online at http://ieeexplore.ieee.org.

Digital Object Identifier 10.1109/TPEL.2015.2508037

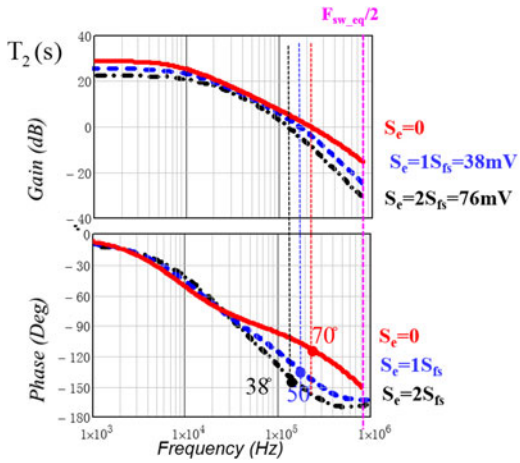

Fig. 3. Impact of external ramp on loop gain bandwidth and phase margin in a two-phase VR example.

between different phases: When the operation range is close to ripple cancellation point, the total inductor current ripple is small and the small amount of current ripple is prone to be disturbed by noise. As a result, external ramp compensation is utilized in commercial products [1], [2] to alleviate the jittering problem caused by the ripple cancellation effect. As shown in Figs. 1 and 2, the external ramp increases the total ramp to compare with control signal and therefore the immunity of the circuit to the disturbing noise is improved.

External ramp compensation is a simple solution to alleviate jittering problem; however, the addition of external ramp affects the dynamic performance. Without changing the compensator parameters, it is observed that the introduction of the external ramp reduces the bandwidth and phase margin of the total loop gain transfer function. One example is shown here with the following parameters: phase number $n_{\rm ph} = 2$; switching frequency $F_{\rm sw} = 800$ kHz/phase, input voltage $V_{\rm in} = 5.2$ V, output voltage $V_o = 2$ V, inductor $L_s = 150$ nH/phase, and output current $I_o = 40$ A. As shown in Fig. 3, without external ramps, the converter is designed with 230 kHz bandwidth and sufficient phase margin (70°). With the external ramp slope around the inductor current falling slope (magnitude of 38 mV), the phase margin reduces to 50° while the bandwidth reduces from 230 to 150 kHz. With external ramp slope around two times the inductor current falling slope, the phase margin further reduces to 38°, which is out of many engineer's comfort zone of at least 45° phase margin.

For quantitative analysis, an accurate small-signal model is indispensable. Several papers. which are closely related to this subject are summarized as follows: In [9], the describing function method is used to derive the transfer function of constant on-time modulator. However, the inductor current information is not included in voltage-mode control structure. For previous small-signal models for constant on-time current-mode control, which includes Redl's analysis based on injected–absorbed current method [10], Ridley's modified average model [11], Vorperian's current-controlled pulsewidth-modulated (PWM) switch model [12], Li's equivalent circuit model based on describing function [7], and Yan's three-terminal switch model [8], none of them includes external ramp compensation as the external ramp is rarely used at that time. In [13]–[20], small-signal analysis for constant on-time V^2 control (or ripple based control) and constant frequency V^2 control with external ramp compensation are presented. However, in V^2 control or ripple-based control structure, not only inductor current ramp but also capacitor voltage ripple participates in modulation. In short, up to now, no good small-signal model for constant on time current-mode control with external ramp compensation is proposed in the literature.

This paper tries to provide a simple and accurate three-terminal switch model for constant on-time current-mode control with external ramp compensation, which will serve as a useful tool for understanding the effect of external ramp and designing feedback control appropriately. The accurate small-signal model will be derived using the describing function method, as this method is becoming popular and has already been successfully applied in PWM buck converters with current-mode control [7], [8] and V^2 control [13]–[20], as well as in more complicated resonant-type converters, such as series resonant converter (SRC) [21]–[23] and *LLC* resonant converters [24], [25]. Besides, a simplified equivalent circuit model is also provided, which is presented in the more preferred circuit form instead of a mathematical equation form and can provide more physical meaning, similar to the unified three-terminal switch model presented in [8] for current-mode control and [18] for V^2 control. This paper is an extension of the original conference paper [26]. The remaining paper is organized as follows: First, the accurate small-signal control-to-output voltage transfer function is derived using the describing function method in Section II. The result is infinite order and accurate up to infinite frequency. In Section III, the infinite-order transfer function is simplified to a polynomial form in order to derive a simple equivalent circuit model. A three-terminal switch model is proposed based on the nonideal current source concept. It is a complete model, which can be used to examine all transfer functions and is accurate up to half of switching frequency. Section IV discusses some important aspects about the proposed three-terminal switch model. Section V extends the three-terminal switch model to multiphase converters. Section VI provides SIMPLIS simulation and experimental results to verify the proposed three-terminal switch model. Section VII summarizes this chapter.

II. Proposed Small-Signal Model Based on Describing Function

To get exact small-signal control to inductor current transfer function, the describing function method is employed. This method is employed previously to derive transfer function for current-mode control in [7]. The structure of constant on-time current-mode control with external ramp compensation when v_c is under perturbation is shown in Fig. 4. The nonlinear constant on-time modulator, which consists of the switches, the inductor current, the comparator with external ramp, and the on-time generator is treated as a single entity. The steady-state waveform and perturbed waveform are shown in Fig. 5. The assumptions of the describing method and derivation steps are exactly same as [7]; therefore, only critical steps are listed in this paper.

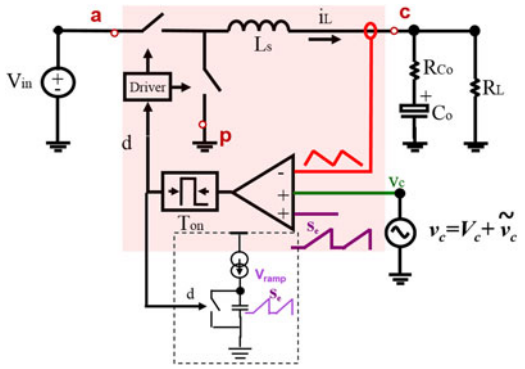

Fig. 4. Modeling method for constant on-time current mode with external ramps.

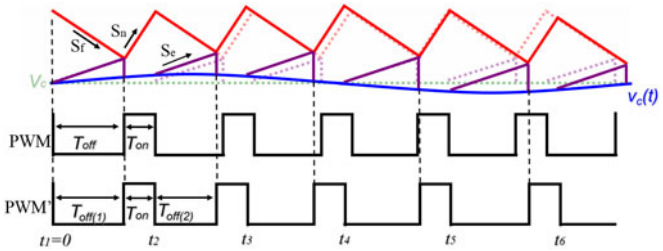

Fig. 5. Steady-state and perturbed waveforms for constant on-time current mode with external ramps.

Step 1: Perturbed off-time calculation shown as follows:

$$v_c(t_{i-1}+T_{\mathrm{off}(i-1)})+s_eT_{\mathrm{off}(i-1)}+s_nT_{\mathrm{on}} = v_c(t_i+T_{\mathrm{off}(i)})+(s_e+s_f)T_{\mathrm{off}(i)} \quad (1)$$

where

$$s_n=R_i\cdot\frac{V_{\mathrm{in}}-V_o}{L_s},\quad s_f=R_i\cdot\frac{V_o}{L_s}.$$

Step 2: Perturbed duty cycle and perturbed inductor current calculation, as shown in (2) and (3)

$$d(t)\big|_{0\le t\le t_M+T_{\mathrm{off}(M)}+T_{\mathrm{on}}} = \sum_{i=1}^{M}\left[u(t-t_i-T_{\mathrm{off}(i)})-u(t-t_i-T_{\mathrm{off}(i)}-T_{\mathrm{on}})\right] \quad (2)$$

$$i_L(t)\big|_{0\le t\le t_M+T_{\mathrm{off}(M)}+T_{\mathrm{on}}} = \int_0^t\left\{\frac{V_{\mathrm{in}}-V_o}{L_s}d(t)-\frac{V_o}{L_s}[1-d(t)]\right\}\cdot dt+i_{L_0}. \quad (3)$$

Step 3: Fourier analysis on inductor current and output voltage to obtain describing function results, as shown in (4) and (5)

$$\frac{i_L(s)}{v_c(s)}=\frac{f_s(1-e^{-sT_{\mathrm{on}}})}{(s_e+s_f)-s_ee^{-sT_{\mathrm{sw}}}}\frac{V_{\mathrm{in}}}{L_ss} \quad (4)$$

$$\frac{v_o(s)}{v_c(s)}=\frac{f_s(1-e^{-sT_{\mathrm{on}}})}{(s_e+s_f)-s_ee^{-sT_{\mathrm{sw}}}}\frac{V_{\mathrm{in}}}{L_ss}\frac{R_L(R_{C_o}C_os+1)}{R_LC_os+1}. \quad (5)$$

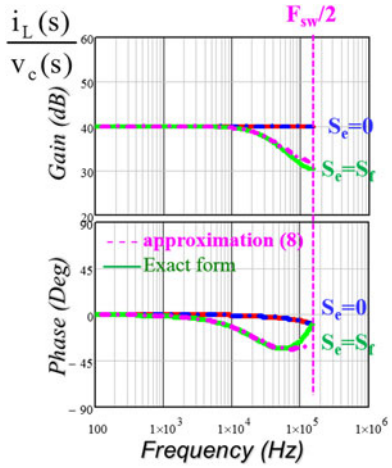

Fig. 6. Comparison of control to inductor current transfer function between approximation (8) and SIMPLIS simulation.

Step 4: Considering the variation of inductor current slopes, the transfer functions from the input voltage to inductor current and output voltage to inductor current are derived in a similar method and the results are shown in (6) and (7)

$$\frac{i_L(s)}{v_{\mathrm{in}}(s)} = \frac{-1}{L_ss}\left[\frac{f_s(1-e^{-sT_{\mathrm{on}}})}{(1-e^{sT_{\mathrm{sw}}})[(s_f+s_e)-s_ee^{-sT_{\mathrm{sw}}}]}\frac{(1-e^{sT_{\mathrm{on}}})}{s\cdot L_s/R_i}\cdot V_{\mathrm{in}}+D\right] \quad (6)$$

$$\frac{i_L(s)}{v_o(s)} = \frac{1}{L_ss}\cdot\left[\frac{f_s(1-e^{-sT_{\mathrm{on}}})}{(s_e+s_f)-s_ee^{-sT_{\mathrm{sw}}}}\cdot\frac{1}{s\cdot L_s/R_i}\cdot V_{\mathrm{in}}-1\right]. \quad (7)$$

III. Proposed Three-Terminal Switch Model

For small duty cycle application, the effect of the dynamic term related to on time in (4) is small and can be neglected. Furthermore, with a first-order polynomial simplification, the infinite-order control-to-inductor transfer function shown in (4) is simplified as follows:

$$\frac{i_L(s)}{v_c(s)}\approx\frac{1}{R_i}\frac{1+(T_{\mathrm{sw}}/2)s}{1+\left(\frac{s_e}{s_f}+\frac{1}{2}\right)T_{\mathrm{sw}}s},\qquad s_f=R_i\cdot\frac{V_o}{L_s}. \quad (8)$$

The approximation is good up to half of switching frequency compared with simulation results, as shown in Fig. 6. If there is no external ramp, the control to inductor current is constant gain, which reveals the fact that in this case the inductor current is well controlled by control signal, or equivalently, the circuit can be regarded as an ideal current source. By adding an external ramp, the gain of control to inductor current drops at high frequency, which reveals the fact that the external ramp reduces the ability of controlling the inductor current, or in other words, the circuit is a nonideal current source due to the effect of external ramp. Based on the physical insight of nonideal current source, an equivalent circuit is derived to represent (8) as Fig. 7.

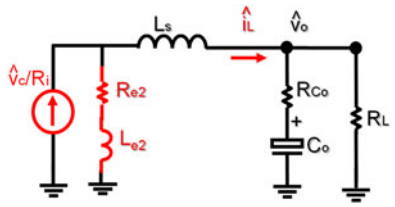

Fig. 7. Equivalent circuit representation of constant on time current-mode control with external ramp compensation for small duty cycle.

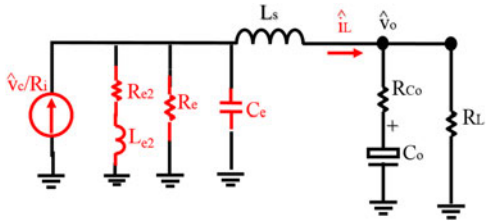

Fig. 8. Equivalent circuit representation of constant on time current-mode control with external ramp compensation for general case.

The expressions of R_{e2} and L_{e2} is shown as follows:

$$R_{e2} = \frac{L_s}{(s_e/s_f)T_{\rm sw}}, \qquad L_{e2} = \frac{L_s}{2(s_e/s_f)}. \tag{9}$$

For general case, the effect of the dynamic term related with on time in (4) may need to be considered: as the duty cycle is large, an additional phase delay is observed. Compared with $D = 0.1$ case, there is additional 33° phase delay at half of the switching frequency for $D = 0.5$ case. Previous equivalent circuit model of constant on time control uses an impedance comprised by R_e and C_e to represent the additional phase delay by forming a pair of double pole whose position is related with on-time [7]. Applying the same concept, the polynomial simplification of control-to-inductor current and its equivalent circuit representation is shown in (10) and Fig. 8, respectively

$$\frac{i_L(s)}{v_c(s)} \approx \frac{1}{R_i}\frac{1+(T_{\rm sw}/2)s}{1+((s_e/s_f)+(1/2))\,T_{\rm sw}s} \frac{1}{1+(s/Q_1\omega_1)+(s/\omega_1)^2}$$
$$Q_1 = \frac{2}{\pi}, \qquad \omega_1 = \frac{\pi}{T_{\rm on}}. \tag{10}$$

The expressions of R_{e2}, L_{e2}, R_e, and C_e are shown as follows:

$$R_e = \frac{2L_s}{((2s_e/s_f)+1)\,T_{\rm on}}, \qquad C_e = \frac{1}{L_s\omega_1^2}$$
$$R_{e2} = \frac{L_s}{(s_e/s_f)(1-D)T_{\rm sw}}, \qquad L_{e2} = \frac{L_s}{2(s_e/s_f)(1-D)}. \tag{11}$$

Fig. 8 can be used to derive control-to-output voltage transfer function and output impedance; however, the input property is lost. To consider the input property and apply the three-terminal switch model concept, the same strategy as used in [8] is adopted. The three-terminal switch model for a single phase is shown in Fig. 9.

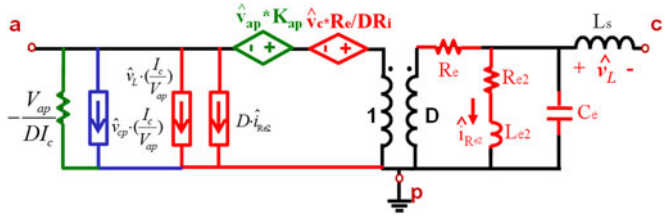

Fig. 9. Three-terminal switch model of constant on-time current-mode control with external ramp compensation.

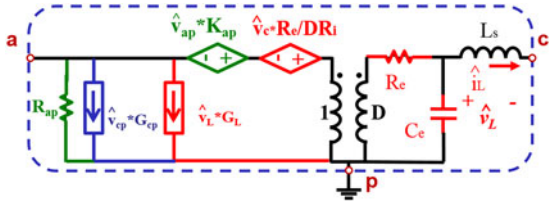

Fig. 10. Proposed three-terminal switch model reduced to original three-terminal switch model in [8] when $S_e = 0$.

The expressions of $K_{\rm ap}$ for constant on-time current-mode control is shown as follows:

$$K_{\rm ap} = \frac{T_{\rm off}}{T_{\rm on}}. \tag{12}$$

IV. Discussion on Proposed Three-Terminal Switch Model

A. Comparison With Previous Three-Terminal Switch Model [8]

As seen from (9), the impedance comprising R_{e2} and L_{e2} is infinite when there is no external ramp; therefore, an additional $R_{e2} - L_{e2}$ branch disappears and the model in Fig. 9(b) reduces to the previous model proposed in [8], as shown in Fig. 10. This means the model shown in Fig. 9(b) is more inclusive and general.

B. Moving Pole and Static Zero Represented by $R_{e2} - L_{e2}$ Impedance

When external ramp increases, the impedance R_{e2} and L_{e2} reduces, and it may shunt part of the current provided by the ideal current source. To illustrate this point, use $S_e = S_f$ as an example. The values of R_{e2} and L_{e2} can be calculated from (9), which is $L_s/(T_{\rm sw})$ and $L_s/2$, respectively. The following analysis shows how R_{e2} and L_{e2} represent the pole and the zero of the circuit shown in Fig. 7. When modulation frequency is low, the impedance of R_{e2} is much larger than L_{e2} and L_s; therefore, the $R_{e2} - L_{e2}$ impedance does not shunt current, all the current flows into L_s branch. The gain is flat, as seen from Fig. 6. When modulation frequency increases, the impedance of inductor L_s branch increases, and the $R_{e2} - L_{e2}$ branch starts to shunt current. The inductor current is determined by an ideal current source coming through a first-order current divider. According to current divider theory, the boundary frequency, which is also the pole position, is the point at which the impedance of

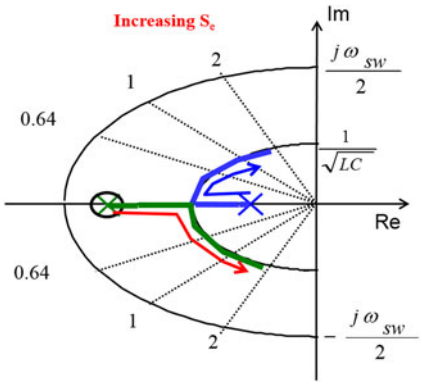

Fig. 11. Pole–zero map of control-to-output voltage transfer function with increasing external ramp.

R_{e2} is the same as the sum impedance of L_{e2} and L_s. For this example, the value is $F_{\rm sw}/(3\pi)$. Now, if the modulation frequency further increases, then impedance of L_{e2} will dominate the $R_{e2}-L_{e2}$ branch and the ratio between this branch and L_s branch is same afterward. This is a zero effect, and the frequency of zero is at $F_{\rm sw}/\pi$. In general, based on the current division theory, due to the branch of $R_{e2}-L_{e2}$, there is a moving pole and a static zero: the pole is determined by R_{e2}, L_{e2}, and L_s, and the zero is determined by R_{e2} and L_{e2}. The expression of the zero and the pole is shown as follows:

$$f_p = \frac{1}{2\pi}\frac{R_{e2}}{L_{e2}+L_s} = \frac{F_{\rm sw}}{\pi(2s_e/s_f+1)}$$
$$f_z = \frac{1}{2\pi}\frac{R_{e2}}{L_{e2}} = \frac{F_{\rm sw}}{\pi}. \tag{13}$$

C. Effect of External Ramp on Pole–Zero Movements and Bode Plots

Previously the effect of $R_{e2}-L_{e2}$ impedance with a given external ramp is discussed: a moving pole and a static zero. Fig. 11 shows the pole–zero map with different external ramp and the following circuit parameters: $F_{\rm sw}=300$ kHz, $V_{\rm in}=12$ V, $V_o=1.2$ V, $L_s=300$ nH, $R_L=100$ mΩ, eight ceramic capacitors (1.4 mΩ/100 μF), and $R_i=10$ mΩ. The ESR zero of the capacitor is far away from the switching frequency and can be ignored. From Fig. 7, when external ramp is zero, $R_{e2}-L_{e2}$ impedance is infinite and only the pole caused by output capacitor and load exists. When external ramp increases, $R_{e2}-L_{e2}$ branch impedance decreases and starts to shunt current in a certain frequency range. As analyzed in previous section, there is a stationery zero located at $F_{\rm sw}/\pi$, which is determined by R_{e2} and L_{e2} and a moving pole, which is determined by R_{e2}, L_{e2}, and L_s, as shown in (13). Further increase the external ramp, the impedance of $R_{e2}-L_{e2}$ branch is so small that the current source is shunt by this branch instead of delivering to the output. This means that the current loop is killed by the large external ramp and the control is turned into voltage mode control. The moving pole combines with the single pole caused by output capacitor and load and forms a pair of double pole at power stage *LC* filter corner frequency.

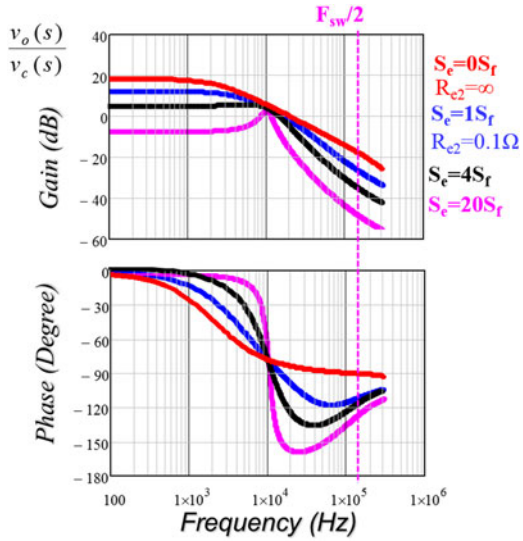

Fig. 12. Bode plots of control to output voltage transfer function with increasing external ramp.

Fig. 12 shows the Bode plots of control to output voltage transfer function with increasing external ramp. When $s_e=0$ (red), only one pole caused by output capacitor and load exists, and it is a first-order circuit as the minimum phase is around $-90°$. When $s_e=1s_f$ (blue), the pole starts to move and split with the zero. When $s_e=20s_f$ (pink), the moving pole combines with the low-frequency pole and forms a double pole at power stage corner frequency; in this case, the current loop effect is killed by the large external ramp, changing the current-mode to voltage-mode control.

D. Comparison with Peak Current-Mode Control and Constant On-Time Voltage-Mode Control

From Figs. 11 and 12, the characteristics of control-to-output voltage transfer function with different external ramps are similar as in the case of constant frequency peak current-mode control. The only difference is caused by the stationery zero, which shows a high-frequency phase boost, shown in Fig. 13. The comparison indicates possible bandwidth improvement with constant on-time current-mode control due to stationery zero.

With a large external ramp, the current loop effect is killed and the circuit turns into voltage-mode control. For constant on-time voltage-mode control, the describing function method is utilized to derive the transfer function of variable-frequency modulation scheme in [9] and the control-to-output voltage transfer function is shown as follows:

$$G_{c2vo\_v} = \frac{DV_{\rm in}}{s_eT_{\rm sw}}\frac{1+R_{C_o}C_os}{1+s/(Q_o\omega_o)+(s/\omega_o)^2}e^{\frac{1-D}{2}T_{\rm sw}s}$$
$$\omega_o = \frac{1}{\sqrt{LC}}, \qquad Q_o \approx R_L\sqrt{\frac{C}{L}}. \tag{14}$$

As shown in Fig. 14, under $s_e=1000\,s_f$ case, control to output voltage transfer function of constant on-time voltage mode agrees very well with constant on-time current mode. There is a slight difference in high-frequency phase due to

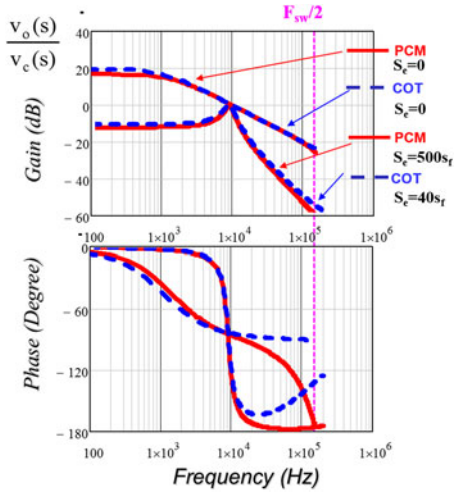

Fig. 13. Control to output voltage Bode plots comparison between constant on-time current mode and peak current mode: (1) $S_e = 0$; (2) $S_e = 500\ S_f$ (PCM) and $S_e = 40\ S_f$ (COT).

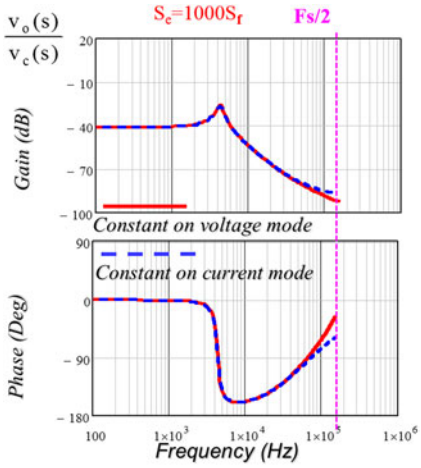

Fig. 14. Control-to-output voltage Bode plots comparison between constant on-time voltage mode and current mode under $s_e = 1000\ s_f$.

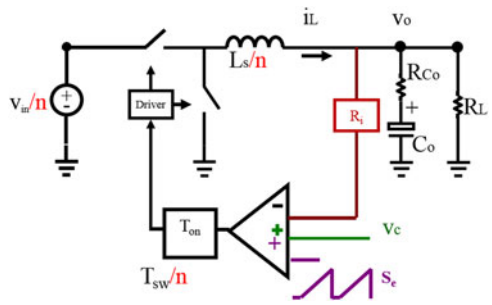

Fig. 15. Equivalent single phase constant on-time current-mode control.

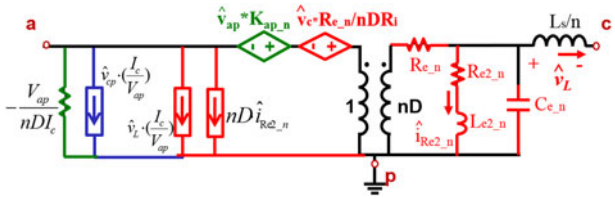

Fig. 16. Complete three-terminal switch model of multiphase constant on-time current-mode control with external ramp compensation.

TABLE I
ANALYTICAL EXPRESSIONS OF TRANSFER FUNCTIONS

$$\frac{\hat{v}_o(s)}{\hat{v}_c(s)} = K_p \frac{1+R_C Cs}{(1+s/\omega_p)\cdot\Delta(s)} \frac{1+(T_{\rm sw}/2)s}{1+((s_e/s_f)+(1/2))\,T_{\rm sw}\,s} \quad (18)$$

$$\frac{\hat{i}_L(s)}{\hat{v}_c(s)} = \frac{K_p}{R_L} \frac{1+R_L Cs}{(1+s/\omega_p)\cdot\Delta(s)} \frac{1+(T_{\rm sw}/2)s}{1+((s_e/s_f)+(1/2))\,T_{\rm sw}\,s} \quad (19)$$

$$\frac{\hat{v}_o(s)}{\hat{v}_{\rm in}(s)} = K_{\rm in} \frac{1+R_C Cs}{(1+s/\omega_p)\cdot\Delta(s)} \frac{1+(T_{\rm sw}/2)s}{1+((s_e/s_f)+(1/2))\,T_{\rm sw}\,s} \quad (20)$$

$$\frac{\hat{i}_L(s)}{\hat{v}_{\rm in}(s)} = \frac{K_{\rm in}}{R_L} \frac{1+R_L Cs}{(1+s/\omega_p)\cdot\Delta(s)} \frac{1+(T_{\rm sw}/2)s}{1+((s_e/s_f)+(1/2))\,T_{\rm sw}\,s} \quad (21)$$

$$\frac{\hat{v}_o(s)}{\hat{i}_o(s)} = R_L \,||(R_{Co} + \frac{1}{C_o s})||(sL_s + \frac{1}{R_e C_e s+1}||(R_{e2} + sL_{e2})) \quad (22)$$

$$\Delta(s) = 1 + \frac{s}{Q_1\omega_1} + \frac{s^2}{\omega_1^2}, \qquad \omega_1 = \frac{\pi}{T_{\rm on}}, \qquad Q_1 = \frac{2}{\pi}$$

$$K_p = \frac{R_L}{R_i(1-k_2/R_i\cdot R_L)}, \qquad K_{\rm in} = \frac{R_L}{(1-k_2/R_i\cdot R_L)} \frac{T_{\rm on}}{2L_s}$$

$$k_2 = -\frac{T_{\rm on}R_i}{L_s} \times \frac{((1/2)+(s_e/Ds_f)) + \left(T_{\rm on}((1/\pi^2)+(1/2D)((1/2)+(s_e/s_f)))\right)s}{1+(T_{\rm sw}/2)s} \quad (23)$$

the first-order polynomial approximation when deriving constant on-time current-mode control while the model shown in (14) use an exponential term to represent the phase boosting phenomenon.

V. EXTENSION TO MULTIPHASE CONVERTERS

To extend the proposed three-terminal switch model to multiphase constant on-time current-mode control case, the summed inductor current signal should be examined carefully as it is the feedback signal to determine the duty cycle. The strategy is to derive an equivalent single-phase converter and then use the equivalent circuit model of single-phase converter. For *n*-phase converter under duty cycle no-overlap case, the rising slope and falling slope for summed inductor current is shown as (15). From small-signal point of view, it is equivalent to the single-phase constant on-time control, as shown in Fig. 15. The equivalent switching frequency is *n* times that of single phase, the inductor is reduced to 1/*n* of the single-phase inductor and the input voltage is also reduced to 1/*n*. Therefore, the equivalent circuit model for multiphase constant on-time current-mode control with external ramp compensation can be derived, as shown in Fig. 16. The expressions of R_{e_n}, C_{e_n}, R_{e2_n}, and L_{e2_n} are shown in (16), and the expressions of pole and zero caused by external ramps are shown in (17). Comparing (16) and (17) with single-phase equations (11) and (13), the pole and zero positions are higher as the equivalent switching frequency is *n* times the switching frequency of single phase

$$s_{n\_n} = R_i\frac{V_{\rm in}-nV_o}{L_s} = R_i\frac{V_{\rm in}/n-V_o}{L_s/n},$$
$$s_{f\_n} = R_i\frac{nV_o}{L_s} = R_i\frac{V_o}{L_s/n} \quad (15)$$
$$R_{e\_n} = \frac{2L_s/n}{((2s_e/s_{f\_n})+1)\,T_{\rm on}}, \qquad C_{e\_n} = \frac{n}{L_s\omega_1^2}$$

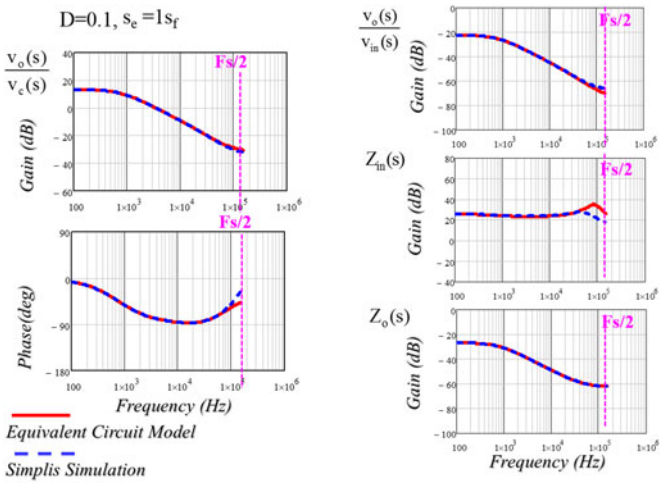

Fig. 17. SIMPLIS verification for single-phase constant on-time current mode with $D = 0.1$ and $S_e = 1\ S_f$.

$$R_{e2\_n} = \frac{L_s}{(s_e/s_{f\_n})(1-nD)T_{\rm sw}},$$
$$L_{e2\_n} = \frac{L_s/n}{2(s_e/s_{f\_n})(1-nD)} \quad (16)$$
$$f_{p\_n} = \frac{1}{2\pi}\frac{R_{e2\_n}}{L_{e2\_n}+L_s/n} = \frac{nF_{\rm sw}}{\pi(2s_e/s_{f\_n}+1)}$$
$$f_{z\_n} = \frac{1}{2\pi}\frac{R_{e2\_n}}{L_{e2\_n}} = \frac{nF_{\rm sw}}{\pi}. \quad (17)$$

VI. Analytical Expressions of Important Transfer Functions for Buck Converters

For easy reference, the analytical expressions for important transfer functions for buck converters are listed in Table I. The transfer functions can be derived easily using circuit analysis techniques from Fig. 9.

VII. Simulation and Experimental Verification

The SIMPLIS simulation tool is used to verify the small-signal analysis. In all the graphs, the "equivalent circuit model" means the model derived from simplified equivalent circuit model shown in Figs. 9 and 16, while "SIMPLIS simulation" means the transfer functions from simulation of the real switching circuit. Fig. 17 shows simulation verification for a single-phase constant on time current-mode control with the following parameters: $F_{\rm sw} = 300$ kHz, $V_{\rm in} = 12$ V, $V_o = 1.2$ V, $L_s = 300$ nH, $R_L = 100$ mΩ, eight OSCON capacitors (6 mΩ/560 μF), $R_i = 10$ mΩ, and $s_e = 1s_f$. All four transfer functions, including control to output voltage, audio susceptibility, output impedance, and input impedance are compared. The results from proposed equivalent circuit model shown in Fig. 9 agrees with simulation results well up to $1/2f_{\rm sw}$ for all transfer functions.

Fig. 18 shows verification of control to output voltage transfer function with different external ramps and 0.1 duty cycle. In all cases, the model agrees well with simulation result up to $1/2f_{\rm sw}$. When the external ramp is large, the circuit changes from first-order current-mode control to second-order voltage-mode control, with a high-frequency phase boost due to the stationery zero.

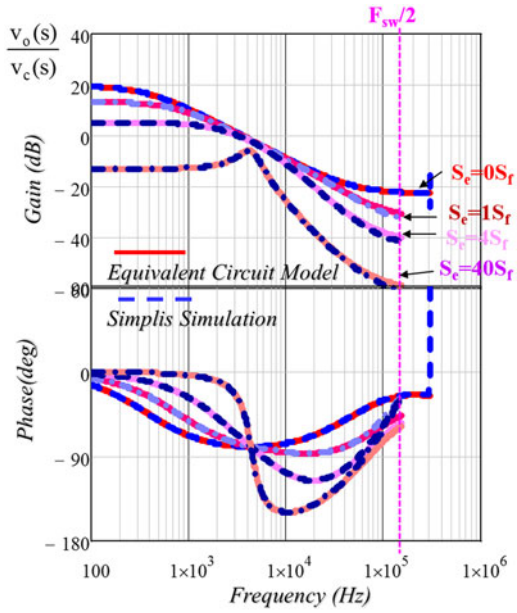

Fig. 18. SIMPLIS verification of control to output voltage transfer function for single-phase constant on time current mode with different external ramps.

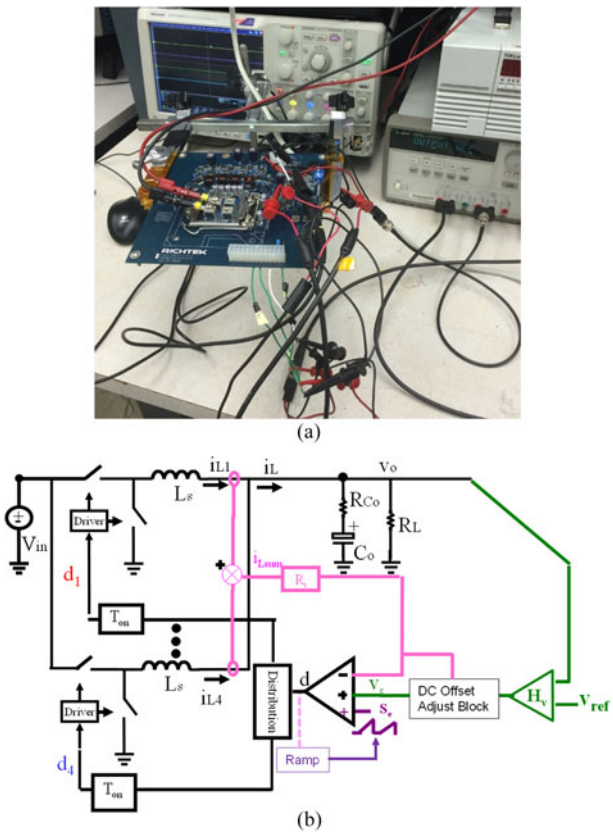

Fig. 19. (a) Experimental setup and (b) simplified diagram for RT8859M Demo Board.

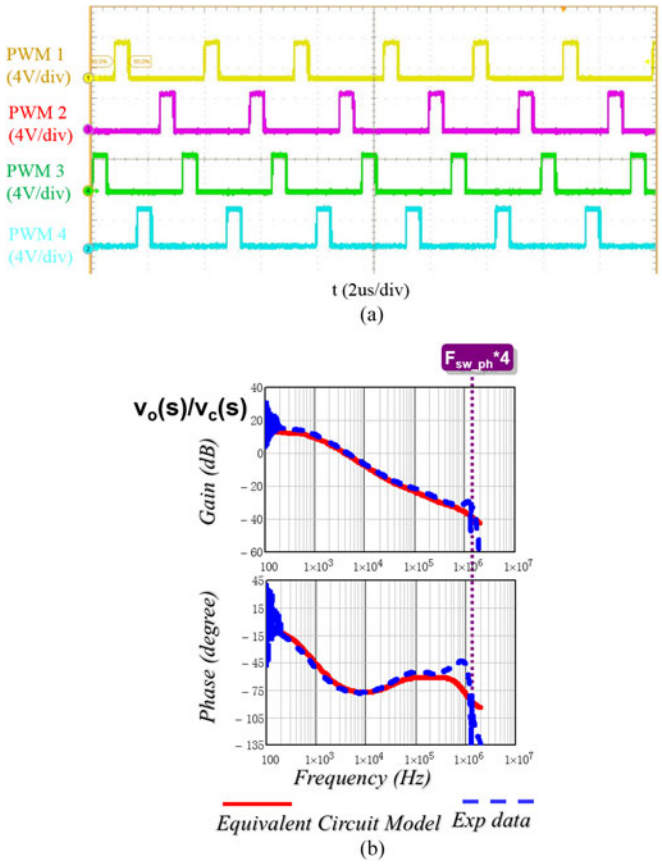

Fig. 20. Experimental verification for case I: $D = 0.2$ ($V_{in} = 6$ V, $V_o = 1$ V): (a) steady-state waveform and jittering performance and (b) verification of control to output voltage transfer function.

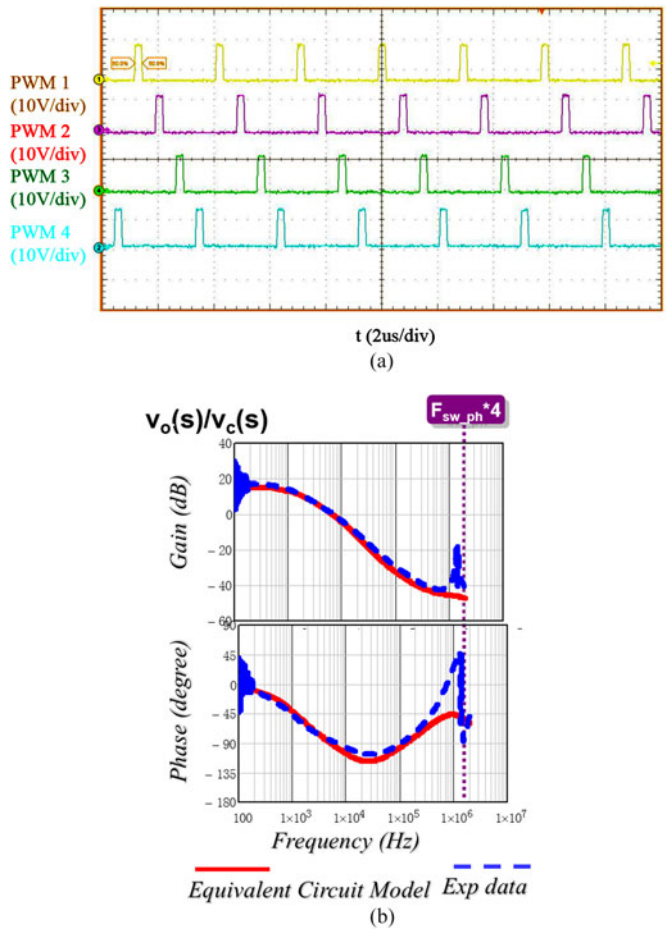

Fig. 21. Experimental verification for case II: $D = 0.1$ ($V_{in} = 12$ V, $V_o = 1$ V): (a) steady-state waveform and (b) verification of control to output voltage transfer function.

Figs. 19–21 show the experimental verification based on demo board of controller RT8859M from Richtek Inc. As shown in Fig. 19(b), a demo board for RT8859M is a four-phase buck converter for CPU power supply with constant on-time current-mode control and external ramp compensation. Two cases are measured and compared based on the demo board.

A. Case I

$V_{\rm in} = 6$ V, $V_o = 1$ V, and $I_o = 4$ A; phase number $n = 4$. For each phase, $D \approx 0.2$, $T_{\rm sw} \approx 315$ kHz, $L_s = 300$ nH; effective current sensing gain $R_i \approx 10$ mΩ; output capacitor: 7 OSCON Caps (560 μF/6 mΩ). The external ramp is implemented inside the controller RT8859M and the magnitude is 133 kV/s, or around 40 mV per switching cycle, which corresponds to around 1.2 S_f in experiment. From Fig. 20(a), although the operating point is around cancellation point, jittering performance is good due to the help of the external ramp. Fig. 20(b) shows verification of control to output voltage transfer function. Compared with measurement data, the equivalent circuit model accurately predicts the small-signal behavior.

B. Case II

The inductor is changed to around 3.3 μH for each phase, the number of output capacitors is reduced from 7 to 5. $V_{\rm in} = 12$ V, $V_o = 1$ V, which corresponds to a duty cycle around 0.1, all other circuit parameters are same as Case I. As shown in Fig. 21, the equivalent circuit model also agrees very well with measurement results. As analyzed in previous sessions, the high-frequency phase boost due to the stationary zero is also observed in measurement.

VIII. Summary and Conclusion

This paper first analyzed the effect of external ramp on small-signal model of constant on-time current-mode control. It is found that external ramp brings additional dynamics by introducing a moving pole and a static zero. Next, a three-terminal switch model is proposed based on nonideal current source concept, where the nonidealness of the current source is presented by a $R_{e2} - L_{e2}$ branch. The equivalent circuit model is an extension of previous unified three-terminal switch model proposed in [8] and can be reduced to constant on time voltage-mode model [9] when external ramp is extremely large. The equivalent circuit model is a complete model and can be used to examine all the transfer functions. Furthermore, the model is extended to multiphase current-mode control and is verified with SIMPLIS simulation and experimental results.

REFERENCES

[1] Texas Instruments. (2011, Dec.). *TPS59650 datasheet* [Online]. Available: http://www.ti.com/product/tps59650

[2] Richtek Cooperation. (2013, Sep.). *RT8859M datasheet* [Online]. Available: http://www.richtek.com/product_detail.jsp?s = 873

[3] B. Sahu, "Analysis and design of a fully-integrated current sharing scheme for multi-phase adaptive on-time modulated switching regulators," in *Proc. IEEE PESC*, 2008, pp. 3829–3835.

[4] C. Cheng, J. Huang, and C. Li, "Circuit and method for constant on-time control for an interleaved multiphase voltage regulator," U.S. Patent 8 159 197 B2, Apr. 2012.

[5] C. W. Deisch, "Switching control method changes power converter into a current source," in *Proc. IEEE Power Electron. Spec. Conf.*, 1978, pp. 300–306.

[6] F. C. Lee, R. A. Carter, and Z. D. Fang, "Investigations of stability & dynamic performances of a current-injected regulator," *IEEE Trans. Aerosp. Electron. Syst.*, vol. AES-19, no. 2, pp. 274–287, Mar. 1983.

[7] J. Li and F. C. Lee, "New modeling approach and equivalent circuit representation for current mode control" *IEEE Trans. Power Electron.*, vol. 25, no. 5, pp. 1218–1230, May 2010.

[8] Y. Yan, F. C. Lee, and P. Mattavelli, "Unified three-terminal switch model for current mode controls," *IEEE Trans. Power Electron.*, vol. 27, no. 9, pp. 4060–4070, Sep. 2012.

[9] J. Sun, "Small-signal modeling of variable-frequency pulsewidth modulators," *IEEE Trans. Aerosp.*, vol. 38, no. 3, pp. 1104–1108, Jul. 2002.

[10] R. Redl and N. O. Sokal, "Current-mode control, five different types, used with the three basic classes of power converters: Small-signal ac and large-signal dc characterization, stability requirements, and implementation of practical circuits," in *Proc. IEEE PESC'85*, pp. 771–785.

[11] R. B. Ridley, "A new continuous-time model for current-mode control with constant frequency, constant on-time, and constant off-time, in CCM and DCM," in *Proc. IEEE PESC'90*, pp. 382–389.

[12] V. Vorperian, "Analysis of current-mode controlled PWM converters using the model of the current-controlled PWM switch," in *Proc. IEEE Power Convers.,* 1990, pp. 183–195.

[13] S. Tian, K. Cheng, F. C. Lee, and P. Mattavelli, "Small-signal model analysis and design of constant on-time V2 control for low-ESR caps with external ramp compensation," in *Proc. IEEE ECCE*, 2011, pp. 2944–2951.

[14] S. Tian, F. C. Lee, P. Mattavelli, K. Y. Cheng, and Y. Yan, "Small-signal analysis and optimal design of external ramp for constant on-time V2 control with multilayer ceramic caps," *IEEE Trans. Power Electron.*, vol. 29, no. 8, pp. 4450–4460, Aug. 2014.

[15] S. Tian, F. C. Lee, P. Mattavelli, and Y. Yan, "Small-signal analysis and design of constant frequency V2 peak control," in *Proc. IEEE APEC*, 2013, pp. 1717–1724.

[16] S. Tian, F. C. Lee, P. Mattavelli, and Y. Yan, "Small-signal analysis and optimal design of constant frequency V2 control," *IEEE Trans. Power Electron.*, vol. 30, no. 3, pp. 1724–1733, Mar. 2015.

[17] S. Tian, F. C. Lee, Q. Li, and Y. Yan, "Unified equivalent circuit model of V2 control," in *Proc. IEEE APEC*, 2014, pp. 1016–1023.

[18] S. Tian, F. C. Lee, Q. Li, and Y. Yan, "Unified equivalent circuit model and optimal design of V2 controlled buck converters," *IEEE Trans. Power Electron.*, vol. 31, no. 2, pp. 1734–1744, Feb. 2016.

[19] K. Cheng, F. Yu, S. Tian, F. C. Lee, and P. Mattavelli, "Digital hybrid ripple-based constant on-time control for voltage regulator modules," in *Proc. IEEE APEC*, 2011, pp. 346–353.

[20] K. Cheng, S. Tian, F. Yu, F. C. Lee, and P. Mattavelli, "Digital hybrid ripple-based constant on-time control for voltage regulator modules," *IEEE Trans. Power Electron.*, vol. 29, no. 6, pp. 3132–3144, Jun. 2014.

[21] E. X. Yang, F. C. Lee, and M. M. Jovanovic, "Small-signal modeling of power electronic circuits by extended describing function concept," in *Proc. Virginia Power Electron. Center Semin.*, 1991, pp. 167–178.

[22] S. Tian, F. C. Lee, Q. Li, and B. Li, " Small-signal equivalent model of series resonant converter," in *Proc. IEEE ECCE*, 2015, pp. 172–179.

[23] S. Tian, F. C. Lee, and Q. Li, "A simplified equivalent circuit model of series resonant converter," *IEEE Trans. Power Electron.*, vol. 31, no. 5, pp. 3922–3931, May, 2016.

[24] S. Tian, F. C. Lee, and Q. Li, "Equivalent circuit modeling of LLC resonant converter," in *Proc. IEEE APEC* 2016, to be published.

[25] S. Tian, "Equivalent circuit model of high frequency PWM and resonant converters," Ph.D. dissertation, *Dept. Elect. Comput. Eng.*, Virginia Tech, Blacksburg, VA, USA, Aug. 2015.

[26] S. Tian, F. C. Lee, J. Li, Q. Li, and P. Liu, "Equivalent circuit model of constant on-time current mode control with external ramp compensation," in *Proc. IEEE ECCE*, 2014, pp. 3747—3754.

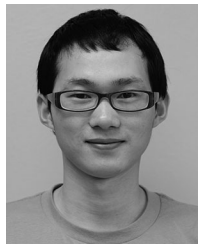

Shuilin Tian (S'11) received the B.S. degree in electrical engineering from Zhejiang University, Hangzhou, China, in 2008, and the M.S. and Ph.D. degrees in electrical engineering from the Center for Power Electronics Systems (CPES), Virginia Tech, Blacksburg, USA, in April 2012 and Aug. 2015, respectively.

He is currently an Applications Engineer in Linear Technology, Milpitas, CA, USA. His current research interests include modeling, analysis, control of PWM converters, and resonant converters.

Fred C. Lee (S'72–M'74–SM'87–F'90–LF'12) received the B.S. degree in electrical engineering from the National Cheng Kung University, Tainan City, Taiwan, in 1968, and the M.S. and Ph.D. degrees in electrical engineering from Duke University, Durham, NC, USA, in 1972 and 1974, respectively.

He is currently a University Distinguished Professor at Virginia Polytechnic Institute and State University (Virginia Tech), Blacksburg, USA, and the Founder and Director of the Center for Power Electronics Systems. He holds 72 U.S. patents and has published 252 journal articles and 639 refereed technical papers.

Dr. Lee was the President of the IEEE Power Electronics Society (1993–1994) and is a recipient of the William E. Newell Power Electronics Award in 1989. He is a Member of the National Academy of Engineering in United States and an academician of Academia in Taiwan.

Jian Li was born in Chengdu, Sichuan, China, in 1978. He received the M.S. degree in control theory and control engineering from Tsinghua University, Beijing, China, in 2004, and the Ph.D. degree from the Center of Power Electronics Systems, Virginia Tech, Blacksburg, VA, USA, in 2009.

He is currently an Applications Engineer Section Leader in Linear Technology, Milpitas, CA, USA. His current research interests include modeling and the digital control techniques for switching mode power supply.

Qiang Li (M'12) received the B.S. and M.S. degrees in power electronics from Zhejiang University, Zhejiang, China, in 2003 and 2006, respectively, and the Ph.D. degree from Virginia Tech, Blacksburg, VA, USA, in 2011.

He is currently an Assistant Professor with the Center for Power Electronics Systems, Virginia Tech. His current research interests include distributed power systems, high-frequency power conversion, and high-density electronics packaging and integration.

Pei-Hsin Liu (S'12) received the B.S. and M.S. degrees in electrical engineering from Taiwan, in 2003 and 2005, respectively, and the Ph.D. degree in electrical engineering from the Center for Power Electronics Systems, Virginia Tech, Blacksburg, VA, USA, in May 2015.

He is currently a System Engineer with the Texas Instruments, Manchester, NH, USA. His current research interests include analysis, modeling, and digital control of power electronic circuits.